Supplemental Material: Spatio-Temporal Coupling Controlled Laser for Electron Acceleration

Lu Wang,[1,*] Uwe Niedermayer,[2] Jingui Ma,[1] Weihao Liu,[3] Dongfang Zhang,[1,†] and Liejia Qian[1]

[1] *Key Laboratory for Laser Plasmas, School of Physics and Astronomy, Shanghai Jiao Tong University, China*
[2] *Technische Universität Darmstadt, Schlossgartenstrasse 8, D-64289 Darmstadt, Germany*
[3] *College of Electronic and Information Engineering, Nanjing University of Aeronautics and Astronautics, China*

Contents

* lu.wangthz@outlook.com
† dongfangzhang@sjtu.edu.cn

I. Analytical expression of the electric field

The electric field in the time domain is defined as $E(x,z,t) = \mathcal{F}[E(x,z,\omega)]$, where $\mathcal{F}$ represents the Fourier transform. The analytical expressions follow the ABCDEF matrix method [1]. The propagation, focusing, and grating matrices are denoted by M_L, M_f, and M_g as the following,

$$M_L = \begin{pmatrix} 1 & L & 0 \\ 0 & 1 & 0 \\ 0 & 0 & 1 \end{pmatrix}, M_f = \begin{pmatrix} 1 & 0 & 0 \\ -1/f & 1 & 0 \\ 0 & 0 & 1 \end{pmatrix}, M_g = \begin{pmatrix} A & 0 & 0 \\ 0 & 1/A & \beta\Delta\omega \\ 0 & 0 & 1 \end{pmatrix}, \tag{S1}$$

where L is the propagation distance, f is the focal length, β is the angular dispersion, $A = \cos(\theta_o)/\cos(\theta_i)$ is the modification factor for grating with grating incidence and output angle defined as θ_i and θ_o respectively. The illustration of the optical system is presented in Fig. S1.

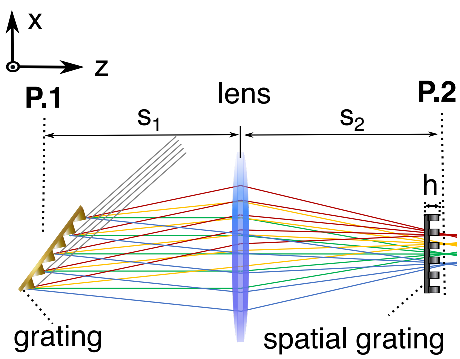

FIG. S1. Illustration of the optical system

With the final ABCDEF matrix defined as

$$M = \begin{pmatrix} A(1-s_2/f) & [s_1(1-s_2/f)+s_2]/A & \beta\Delta\omega\,[s_1(1-s_2/f)+s_2] \\ -A/f & (1-s_1/f)/A & \beta\Delta\omega(1-s_1/f) \\ 0 & 0 & 1 \end{pmatrix} = M_L(s_2)M_fM_L(s_1)M_g, \tag{S2}$$

and the $q_1 = i\pi\sigma_1^2/\lambda_0$, one can obtain the electric field as the following:

$$q_2 = (M_{11}q_1 + M_{12})/(M_{21}q_1 + M_{22}), \tag{S3}$$

$$A_2 = A_1\sqrt{1/(M_{11} + M_{12}/q_1)}, \tag{S4}$$

$$E(x, s_1+s_2, \omega) = \frac{A_2}{\sqrt{2\pi}} \exp(-\frac{ik(x-M_{13})^2}{q_2}) \exp(-iM_{23}kx) \exp(-\frac{\tau^2\Delta\omega^2}{4}) \times \exp\left[i(\frac{1}{2}\Phi_2\Delta\omega^2 + \frac{1}{6}\Phi_3\Delta\omega^3)\right], \tag{S5}$$

where the subscripts on M indicate the matrix element in Eq. (S2) and the wavevector $k = 2\pi/\lambda_0$. Note that Eq. (S5) is the electric field without any effect of the acceleration structure. The effect of the acceleration structure is considered by introducing a periodic delay, where the period is calculated interactively with the electron velocity. Before interacting with the acceleration structure, the electric field propagates through distance $f - h$ between the lens and the spatial grating. We found that the extra propagation distance h has minor influence on acceleration results with our parameters since $f \sim$ cm and $h \sim \mu$m.

In our case, we choose the Littrow configuration for the grating at **P.1**. Consequently $\theta_i = \theta_o$ and $A = 1$. With the conditions $A = 1$ and $s_1 = s_2 = f$, Fig. S1 reduces to Fig. 1**a** in the main text and Eq. (S5) reduces to Eq. (2) in the main text. The parameters used in the main text and this supplementary are listed below in Table I. Note that τ represents the transform limited pulse duration at **P.1**, the parameters at **P.2** are denoted with a prime.

TABLE I. Parameters

Name	values
focal length f	100 mm
modification factor A	1
incidence beam size σ_1	6 mm
center wavelength λ_0	10 μm
spatial grating thickness h	2 μm
gap distance l	1 um
refractive index of spatial grating (n_{Si})	3.5 [2]
transform limited pulse duration τ_{FWHM}	100 fs
τ	$\tau_{\mathrm{FWHM}}/\sqrt{2\ln(2)}$
total input energy	0.48 mJ
perfectly matched (main text Fig. 2) 0.1 eV	$\Phi_2 = 3.9\times10^{-2}\mathrm{ps}^2$, $\Phi_3 = 1.1\times10^{-3}\mathrm{ps}^3$ $\tau\prime_{\mathrm{FWHM}} = 460$ fs $\sigma\prime_{\mathrm{FWHM}} = 0.16$ mm $\beta = -5.0\times10^{-17}$ s $E_0 = 2\times2.4$ GV/m evanescent coefficient 0.7
realistic (main text Fig. 3,4) 20 keV	$\Phi_2 = 4.5\times10^{-2}\mathrm{ps}^2$, $\Phi_3 = 9.4\times10^{-4}\mathrm{ps}^3$ $\tau\prime_{\mathrm{FWHM}} = 500$ fs $\sigma\prime_{\mathrm{FWHM}} = 0.16$ mm $\beta = -5.4\times10^{-17}$ s $E_0 = 2\times2.25$ GV/m evanescent coefficient 0.3-0.7

To give guidance to future related experiments, the Φ_2 and Φ_3 can be adjusted via a Dazzler. The 10 μm laser could be generated via an OPCPA system [3, 4]. The angular dispersion β can be induced by grating, grating pairs or prism, and the choice of methods to introduce angular dispersion doesn't influence the outcome of the STC scheme we propose.

II. Pulse duration of the STC scheme

One can obtain the electric field distribution in time by Fourier transform Eq. (S5). For the STC scheme, if both the Φ_2 and Φ_3 are zero, the PFT at **P.2** is zero. The PFT is mainly dominated by Φ_2. The Φ_3 brings in small modifications based on the effects from Φ_2. It is challenging to obtain an analytical form of $E(x,z,t)$ when Φ_3 is present. However, the analytical result for $\Phi_3 = 0$ could also bring insights into this problem. The analytical electric field in the time domain (Fourier transform of Eq. (S5) can be written as the following:

$$\mathcal{F}[E(x,2f,\omega)|_{\Phi_3=0}] \propto \exp(i\omega_0 t)\exp\left\{\frac{-Q\left[t+\beta k^2\sigma_1^2 x\Phi_2/(2fQ)\right]^2}{4Q^2+\Phi_2^2}\right\}\exp\left(\frac{-x^2\tau^2k^2\sigma_1^2}{8Qf^2}\right)$$
$$\times\exp\left\{\frac{i[\Phi_2(k^4\sigma_1^4\beta^2x^2/f^2-t^2)/2+2t\beta k^2\sigma_1^2xQ/f]}{4Q^2+\Phi_2^2}\right\}, \tag{S6}$$

where $Q = \tau^2/4+\beta^2k^2\sigma_1^2/2$. In our case the $\beta<0$ is used. Consequently, Φ_2 needs to be positive since larger t represents later arrival time at **P.2**. One can also choose β with positive values combined with a negative Φ_2. With such combinations, one can see from Eq. (S6) that the $x>0$ regime of the pulse arrives later than $x<0$ regime. It can be seen from the second exponential term in Eq. (S6) that the PFT angle is $\tan(\theta) = ck^2\sigma_1^2\beta\Phi_2/2fQ$. Additionally, the pulse duration and the beam size at the focal point are

$$\tau\prime_{\mathrm{FWHM}} = 2\sqrt{2\ln(2)\left(Q+\frac{\Phi_2^2}{4Q}\right)},\quad \sigma\prime_{\mathrm{FWHM}} = 2f\sqrt{\ln(2)\left(\frac{\lambda_0^2}{4\sigma_1^2\pi^2}+\frac{2\beta^2}{\tau^2}\right)}. \tag{S7}$$

Note that since β corresponds to the angular spread, larger β always leads to larger beam size at **P.2**. On the other hand, the pulse duration $\tau\prime_{\mathrm{FWHM}}$ at **P.2** doesn't has a linear relation with β as shown in Eq. (S7). The β corresponds to the minimum pulse duration is written as:

$$\beta_{\mathrm{min}} = \frac{-c}{\omega_0\sigma_1}\sqrt{\Phi_2 - \frac{\tau^2}{2}}. \tag{S8}$$

Note that though Eq. (S8) is the analytical expression derived with $\Phi_3 = 0$, the $\tau\prime_{\mathrm{FWHM}}$ is very close to the value at the center of the beam $x = 0$ for the $\Phi_3 \neq 0$ case with the parameter choices in Table I. In the following contents unless stated otherwise, all the results are presented with parameters for the "realistic (20 keV)" case as shown in Table I. In the main text, the β is set to equal to β_{min}, where β_{min} corresponds to the minimum pulse duration $\tau\prime_{\mathrm{FWHM}}$ at the center of the pulse ($x = 0$). To compare the STC and the PFT schemes, the beam size and the pulse duration of the two schemes are set to be the same at **P.2**. With all the other parameters fixed, the $\tau\prime_{\mathrm{FWHM}}$ versus β is presented in Fig. S2, where the β_{min} is the value expressed in Eq. (S8). In Fig. S2(b), the local pulse duration versus x is presented. It can be seen that due to the TOD, the pulse duration varies along x. The pulse duration at the peak fluence location (center of the pulse $x = 0$) is indicated by a black dashed line.

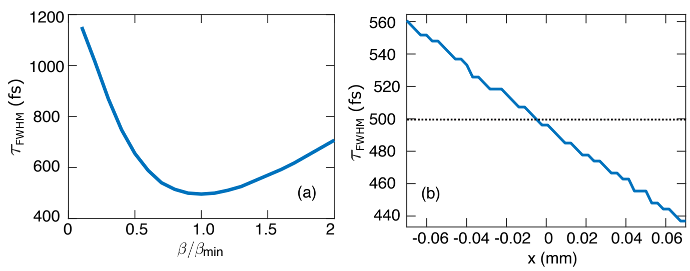

FIG. S2. With the parameters of the "realistic" case in Table 1, the pulse duration (FWHM) at P.2 versus β is presented in (a). β_{mim} represents the value in Eq. (S8). (b) shows the pulse duration change along x with $\beta = \beta_{\mathrm{min}}$. The small wiggles of the pulse duration for STC schemes are the numerical artifacts, since it is calculated numerically.

III. Comparison between the STC and PFT schemes

To scrutinize into the differences of the STC scheme and the PFT scheme, in this section we analyze the local intensity peak and carrier envelope phase of the two schemes (see Fig. S3). It can be seen that the PFT has a linear phase change along the envelope while the STC scheme has a curved phase change.

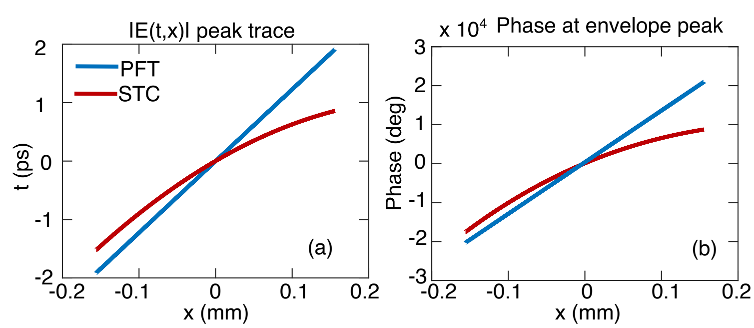

FIG. S3. Comparison between the TPF and STC schemes. (a) shows the arrival time of the intensity peak as a function of x. (b) shows the carrier envelope phase at the intensity peak.

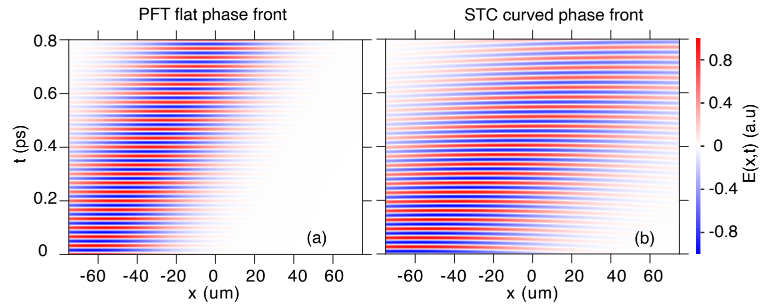

FIG. S4. The phase fronts of the PFT and the STC schemes before interacting with the acceleration structures are presented in (a) and (b), respectively. It can be seen that the STC scheme possesses a curved phase front.

Figure S4 presents the electronic field of the STC and PFT schemes before interacting with the acceleration structure. It indicates that the PFT scheme has a flat phase front whereas the STC scheme has a curved phase front.

In figure S5(a,b), the intensity distributions ($|E(x,t)|^2$) are shown, where x_c denotes the position of the pulse center i.e. peak fluence location. The local pulse duration at three different positions $x_c - 0.45\sigma\prime_{\mathrm{FWHM}}$, x_c and $x_c + 0.45\sigma\prime_{\mathrm{FWHM}}$ are shown in Fig. S5(c-e), respectively. It can be seen that for the PFT scheme, the pulse duration remain unchanged along x, whereas for the STC scheme, the pulse duration varies. This is consistent with Fig. S2(b).

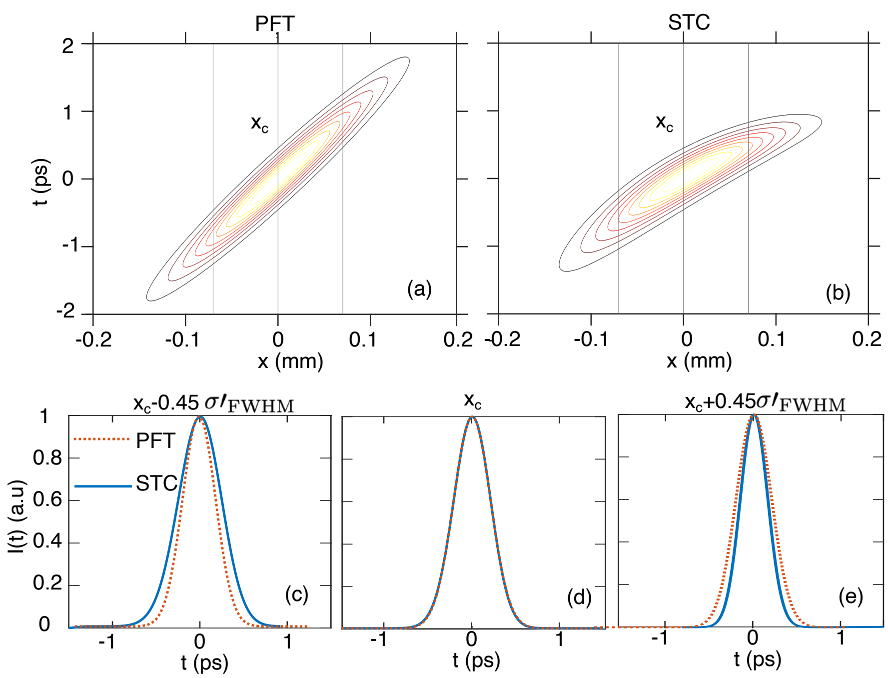

FIG. S5. The intensity for the PFT and STC shemes are presented in **a** and **b**, respectively. The x_c denotes the position of the pulse center i.e. peak fluence location. The local pulse duration at three different positions (vertical lines) $x_c - 0.45\sigma\prime_{\mathrm{FWHM}}$, x_c and $x_c + 0.45\sigma\prime_{\mathrm{FWHM}}$ are shown in **c**, **d**, and **e**, respectively.

IV. Perfectly phase-matched pulse

Here we present the ideal situation where the design of the DLA leads to a perfectly matching field to the electron. In other words, we assume that along the electron acceleration direction x, the electric field is always the local minimum. The acceleration results are presented in Fig. S6. It can be seen that compared to the PFT scheme, the STC scheme leads to larger energy gain and longer interaction length.

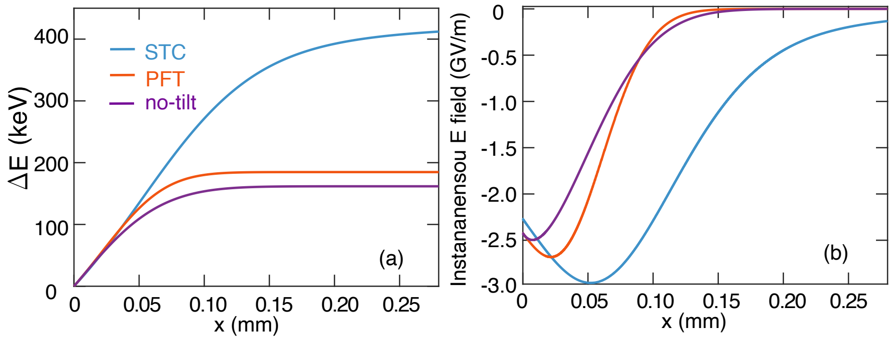

FIG. S6. The kinetic energy gain and the instantaneous field strength are shown in (a) and (b) respectively.

V. Numerical method

To test the convergence of the code, we export the E field of the STC scheme along x (as shown in Fig. 4(b) in the manuscript) to ASTRA. The accelerated results produced by ASTRA is in good agreement with our result as shown in Fig. S7.

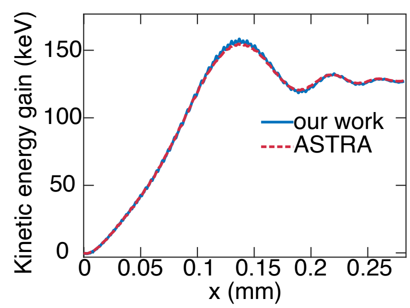

FIG. S7. Comparison of our numerical method with ASTRA.

VI. Different electron initial energy

Here we extend our studies to different initial electron kinetic energies. In addition to the results in the main text (20 keV), acceleration with electron initial energies as 50 keV and 100 keV are shown in Fig. S8(b,c), respectively.

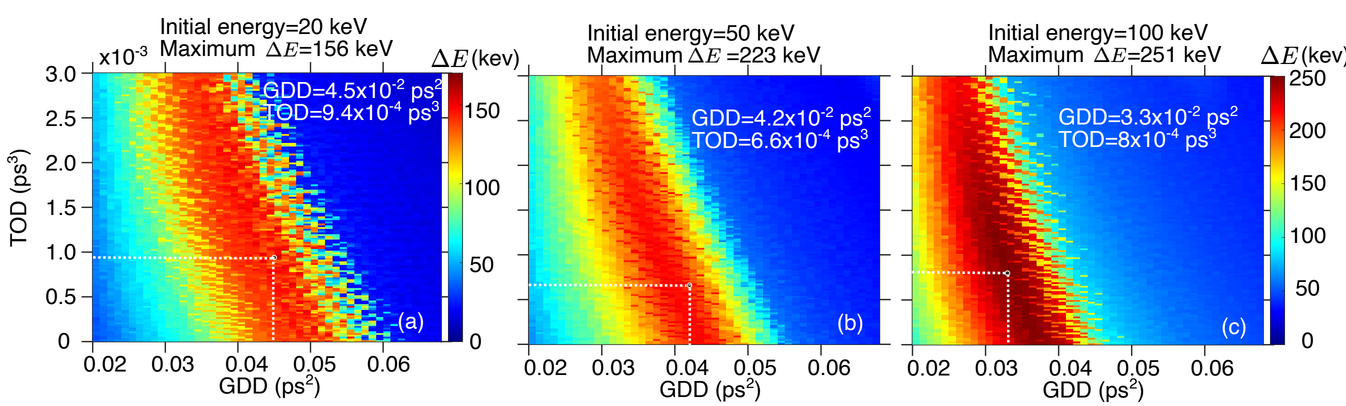

FIG. S8. Acceleration results with different initial energies. The (b) and (c) share the same color bar.

It can be seen that as the increase of the initial electron energy, the GDD required reduces, which corresponds to a decreasing PFT angle.

[1] O. E. Martinez, IEEE journal of quantum electronics **24**, 2530 (1988).
[2] C. D. Salzberg and J. J. Villa, JOSA **47**, 244 (1957).
[3] D. Sanchez, M. Hemmer, M. Baudisch, S. Cousin, K. Zawilski, P. Schunemann, O. Chalus, C. Simon-Boisson, and J. Biegert, Optica **3**, 147 (2016).
[4] S. Qu, H. Liang, K. Liu, X. Zou, W. Li, Q. J. Wang, and Y. Zhang, Optics letters **44**, 2422 (2019).